Chemical Geology

Metal recycling tracked by mercury and helium isotopes in platinum–palladium nuggets from Córrego Bom Sucesso, Brazil
--Manuscript Draft--

Abstract:	The enigmatic botryoidal nuggets of platinum (Pt) and palladium (Pd) from Córrego Bom Sucesso in the southern Serra do Espinhaço, Minas Gerais, Brazil, are considered to have formed during supergene alteration of placer deposits. This is inconsistent with Pt–Os age of 180 Ma that entails formation at depth. Here we report the first mercury (Hg) and helium (He) isotopic determinations of Pt–Pd nuggets. Mercury isotopic compositions have a mass-independent fractionation (MIF) signature with an odd-mass deficit (Δ199Hg -0.22 ± 0.04; 1SD, n = 15), which requires aqueous photochemical reduction of Hg (II). Extremely low 3He/4He (< 0.001 Ra) and extremely high concentrations of He (up to 1.9 x 1017 at/g) are indicative of nugget formation from He-enriched fluids within the quartzite sequence of the Espinhaço basin, not from meteoric surface water. The data are consistent with a nugget-forming setting in the deep biosphere, as a result of groundwater interaction with Pt–Pd–Hg minerals in Pan-African-Brasiliano post-orogenic veins. We propose that the negative Hg-MIF signature was inherited from the vein minerals that originally acquired their Hg from Earth's surface during the intracratonic sedimentation of the Proterozoic Espinhaço basin.

1   **Metal recycling tracked by mercury and helium isotopes in platinum–palladium nuggets**

2   **from Córrego Bom Sucesso, Brazil**

3

4   Alexandre Raphael Cabral[1,2], Changzhou Deng[3], Runsheng Yin[3], Olga V. Yakubovich[4,5],

5   Finlay M. Stuart [6], Miguel Tupinambá[7], Bernd Lehmann[8]

6

7   [1] Centro de Pesquisa Professor Manoel Teixeira da Costa, Instituto de Geociências, Universidade Federal de

8   Minas Gerais (UFMG), Belo Horizonte, MG, 31270-901, Brazil.

9   [2] Centro de Desenvolvimento da Tecnologia Nuclear (CDTN), Belo Horizonte, MG, 31270-901, Brazil.

10   [3] State Key Laboratory of Ore Deposit Geochemistry, Institute of Geochemistry, Chinese Academy of Sciences,

11   Guiyang 550081, China

12   [4] Saint Petersburg State University, Institute of Earth Sciences, Unversitetskaya emb. 7/9, 199034, Saint-

13   Petersburg, Russia

14   [5] Institute of Precambrian Geology and Geochronology RAS, Makarova emb. 2, 199034, Saint-Petersburg,

15   Russia

16   [6] Scottish Universities Environmental Research Centre, Rankine Avenue, East Kilbride G75 0QF UK

17   [7] Tektos-Geotectonic Research Group, Faculdade de Geologia, Universidade do Estado do Rio de Janeiro,

18   20550-050, Rio de Janeiro-RJ, Brazil

19   [8] Mineral Resources, Technische Universität Clausthal, Adolph-Roemer-Str. 2a, 38678 Clausthal-Zellerfeld,

20

21   **Abstract**

22   The enigmatic botryoidal nuggets of platinum (Pt) and palladium (Pd) from Córrego Bom

23   Sucesso in the southern Serra do Espinhaço, Minas Gerais, Brazil, are considered to have

24   formed during supergene alteration of placer deposits. This is inconsistent with Pt–Os age of

25   180 Ma that entails formation at depth. Here we report the first mercury (Hg) and helium (He)

26   isotopic determinations of Pt–Pd nuggets. Mercury isotopic compositions have a mass-

27   independent fractionation (MIF) signature with an odd-mass deficit (Δ^{199}Hg -0.22 ± 0.04; 1SD,

28   n = 15), which requires aqueous photochemical reduction of Hg (II). Extremely low ^{3}He/^{4}He

29 (< 0.001 R_a) and extremely high concentrations of He (up to 1.9×10^{17} at/g) are indicative of

30 nugget formation from He-enriched fluids within the quartzite sequence of the Espinhaço basin,

31 not from meteoric surface water. The data are consistent with a nugget-forming setting in the

32 deep biosphere, as a result of groundwater interaction with Pt–Pd–Hg minerals in Pan-African-

33 Brasiliano post-orogenic veins. We propose that the negative Hg-MIF signature was inherited

34 from the vein minerals that originally acquired their Hg from Earth's surface during the

35 intracratonic sedimentation of the Proterozoic Espinhaço basin.

36

37 **1. Introduction**

38   Platinum was sourced from nuggets in placer deposits until the first quarter of the 20th

39 century, prior to the discovery of lode deposits in South Africa and Siberia (e.g., Hattori and

40 Cabri, 1992). The long-standing debate on the origin of Pt nuggets in regoliths and placer

41 deposits show no sign of being convincingly resolved. The two prevailing mechanisms explain

42 their origin either as residual grains inherited from a magmatic source (e.g., Hattori and Cabri,

43 1992; Oberthür et al., 2017) or authigenic aggregates formed at the surface (e.g., Cousins and

44 Kinloch, 1976; Aiglsperger et al., 2017; Bowles and Suárez, 2021). The placer deposits of

45 Córrego Bom Sucesso, southern Serra do Espinhaço, Minas Gerais, Brazil (Fig. 1), are

46 historically important by providing the nuggets where Pd was first identified (Wollaston, 1809;

47 Hussak, 1906; Cassedanne and Alves, 1992; Cabral et al., 2009). The delicate botryoidal habit

48 and the chemical composition distinguish these nuggets from Pt-rich nuggets of magmatic

49 origin based on the enrichment in Se, Pd and Hg, the virtual absence of Fe and low Ru, Rh, Os

50 and Ir concentrations (Cabral et al., 2019).

51   Mercury isotopes have been used to retrieve geochemical pathways of Hg in modern

52 surface environments (Blum et al., 2014) and in the geological past, from the incorporation of

53 atmospheric Hg into sediments and hydrated oceanic crust, through subduction and

54 dehydration, to the formation of Hg-bearing mineral deposits in volcanic arcs (e.g., Deng et al.,

2021). This relies on mass-independent-fractionation (MIF) signals that were generated at Earth's surface and survived deep geological processes. Significant MIF of odd-mass-number isotopes of Hg (Δ^{199}Hg and Δ^{201}Hg) is commonly observed at Earth's surface – i.e., in soil/sediment, water, atmosphere and biological samples (Blum et al. 2014). Experiments have demonstrated that the signature results from the photoreduction of Hg(II) and photodegradation of methylmercury in aqueous solutions with dissolved organic matter (Bergquist and Blum, 2007). Other processes such as evaporation of Hg^0 (Estrade et al., 2009) and dark abiotic reduction of Hg(II) by dissolved organic matter (Zheng and Hintelmann, 2010) can generate MIF of odd-mass Hg isotopes, but the fractionation is too small to explain the Hg-MIF of natural samples (Blum et al., 2014; Blum and Johnson, 2017).

Helium isotopes are a powerful tool for understanding the source of volatiles in hydrothermal minerals (e.g., Stuart et al., 1994), being particularly suitable for studies of Pt nuggets given the extreme retentivity for He (Shukolyukov et al., 2012a). A supergene origin for mineral aggregates requires the precipitation from meteoric solutions which would have a diagnostic isotopic fingerprint, in contrast to the ^{3}He/^{4}He of crust- and mantle-derived fluids (e.g., Mamyrin and Tolstikhin, 1984). Further, the production of cosmogenic ^{3}He at Earth's surface provides a way to determine the residence time of Pt nuggets in the upper few metres (Yakubovich et al., 2019).

Here we report the Hg and He isotopic compositions of Pt–Pd nuggets from the placer deposit of Córrego Bom Sucesso that have a putative supergene origin (Cabral et al., 2019; Reith et al., 2019), representing the most spectacular case of Pt–Pd neoformations at the Earth's surface. This view has recently been disputed on the basis of Pt–Os age of ca. 180 Ma and Se isotopes, which suggest nugget formation in the deep biosphere (Cabral et al., 2021). The Δ^{199}Hg and Δ^{201}Hg signals and reconnaissance He isotopic determinations provide new constraints on the geochemical processes responsible for the generation of the nuggets. Our

80   novel approach implies that precious-metal nuggets can be used as tracers of metal recycling

81   and fluid interaction in the crust.

82

83   **2. Samples and geological setting**

84   Botryoidal Pt–Pd nuggets were recovered from a heavy-mineral concentrate from

85   Córrego Bom Sucesso, southern Serra do Espinhaço, Minas Gerais, Brazil (Fig. 1, 2) Córrego

86   Bom Sucesso is a stream, with associated placer deposit, in the platiniferous Au–Pd belt of

87   Minas Gerais approximately 50 km SSE of Diamantina (Fig. 1; Cabral et al., 2009). The

88   platiniferous alluvium was deposited on a bedrock of Mesoproterozoic quartzite in the

89   interstices among quartzite boulders, and consists mostly of quartz sand with subordinate

90   specular hematite, tourmaline, tourmalinite fragments, and minor palladiferous gold, Pt–Pd

91   alloy, hongshiite (PtCu) and potarite (PdHg), among other minerals (Cassedanne et al., 1996;

92   Cabral et al., 2017).

93   Platinum–osmium age determinations of 5 nuggets are indistinguishable within error

94   (181 ± 6 Ma; Cabral et al., 2021). The age coincides with the final stage of rapid exhumation

95   that brought basement granite-gneissic rocks to ~70°C until the Eocene–Oligocene (Amaral-

96   Santos et al., 2019). The nugget Pt–Os age coincides with the emplacement of Transminas

97   dolerite dykes that occur in the study area (Cabral et al., 2021) and in south-eastern Brazil,

98   related to the South Atlantic opening (Chaves and Correia Neves, 2005).

99   Hematite-bearing quartz veins cross-cut quartzite of the 1.19-Ga Sopa-Brumadinho

100   Formation of the Espinhaço Supergroup (Chemale et al., 2012) in the Córrego Bom Sucesso

101   catchment. Such veins contain palladiferous gold and a variety of hydrothermal Pt, Pd and Hg

102   minerals, e.g., potarite, hongshiite and jacutingaite (Pt_2HgSe_3) (Cabral et al., 2009, 2017). The

103   veins likely formed after the compressional period of the Brasiliano orogeny (e.g., Cabral et al.,

104   2017), which represents the assembly of West Gondwana (Alkmim et al., 2017, and references

105   therein). Two geodynamic models have been proposed for the formation of Brasiliano orogenic

4

106 domain in the southern Serra do Espinhaço (the Araçuaí orogen): (i) a subduction–collision

107 model in which subduction of oceanic crust occurred between 630 and 580 Ma (e.g., Alkmim

108 et al., 2017); (ii) an intracontinental (ensialic) model (e.g., Fossen et al., 2020). The Brasiliano

109 orogenic event occurred between 620 and 500 Ma in the southern part of the platiniferous Au–

110 Pd belt (Cabral et al., 2020). Quartz veins, with and without Au–Pd–Pt mineralisation, are late

111 in relation to the main orogenic compression, usually regarded as post-orogenic lodes (e.g.,

112 Cabral et al., 2017).

113

114 **3. Methods**

115 *3.1. Mercury isotopes*

116 Total Hg concentrations (THg) and Hg isotopic compositions were determined at the

117 Institute of Geochemistry, Chinese Academy of Sciences. Fifteen Pt–Pd nuggets of 5–19 mg

118 were digested in a water bath (95°C) using 5 mL of aqua regia (HCl:HNO$_3$=3:1). After digestion,

119 THg was measured in solutions by cold vapour atomic absorption spectrometry (F732−S

120 spectrophotometer, Huaguang Ltd, China). Measurements of reference material, GSS-4 (soil),

121 yielded Hg recoveries of 93 and 113%, and coefficients of variation for triplicate analyses were

122 < 9%. The digestion solutions were diluted to 1.0 ng/mL Hg with ~10% acid prior to isotopic

123 analysis using a ThermoFisher Neptune Plus multi-collector inductively coupled plasma mass

124 spectrometer (Yin et al., 2016). Mercury isotopic compositions are reported following

125 convention (Blum and Bergquist, 2007), mass-dependent fractionation expressed in δ^{202}Hg

126 notation, in per mil, referenced to the NIST-3133 Hg standard analysed before and after each

127 sample:

128 $$\delta^{202}\text{Hg}(‰)= [(^{202}\text{Hg}/^{198}\text{Hg}_{sample})/(^{202}\text{Hg}/^{198}\text{Hg}_{standard}) - 1]\times 1000$$

129 Mass-independent fractionation is reported in Δ notation, which describes the difference

130 between the measured δ^{xxx}Hg and the theoretically predicted δ^{xxx}Hg value, in per mil:

5

131
$$\Delta^{xxx}Hg \approx \delta^{xxx}Hg - \delta^{202}Hg \times \beta$$

132 β is equal to 0.2520 for ^{199}Hg, 0.5024 for ^{200}Hg, and 0.7520 for ^{201}Hg. The analytical uncertainty

133 is estimated based on replication of the NIST-3177 standard solution, and full procedural

134 analyses of GSS-4. The overall average and uncertainty of NIST-3177 and GSS-4 (Table 1)

135 agree well with previous studies (Blum and Bergquist, 2007; Deng et al., 2021). The higher

136 2SD uncertainty for either GSS-4 or NIST-3177 are used in calculation of analytical

137 uncertainties.

138

139 *Helium isotopes*

140 Analysis of the Córrego Bom Sucesso nuggets was similar to detrital grains reported

141 previously (Yakubovich et al. 2019). Grains were weighed then placed into 3-mm holes in a

142 previously degassed copper pan, and covered with a degassed sapphire disk and baked for ~36

143 hours at ~150°C in ultra-high vacuum. Helium was extracted by directly heating each nugget

144 with a focused beam of an 808-nm diode laser (Stuart et al., 1999). Quantitative release of He

145 from metals requires melting (Shukolyukov et al., 2012a). This was achieved by slowly

146 increasing laser power (maximum 75W) until melting, then holding for 5 minutes. Active gases

147 were purified by exposure to two SAES GP50 getters and the heavy noble gases were removed

148 by exposure to the liquid-nitrogen-cooled charcoal. The He isotopic composition was

149 determined in a modified ThermoFisher Helix-SFT mass spectrometer (Carracedo et al., 2019).

150 Sensitivity and mass fractionation were obtained by repeated measurements of aliquots of He

151 from a tank of the HESJ standard (Matsuda et al., 2002). The reproducibility of ^{3}He and $^{3}He/^{4}He$

152 measurements was better than 5 per mil over the period of analysis. A Pt foil was melted in

153 order to determine a representative hot blank level to correct the He concentrations released by

154 heating the Pt–Pd nugget. The averages of ^{3}He and ^{4}He blanks were 1.5 x 10^4 atoms and 7 x

155 10^8 atoms, respectively.

156   Palladium alloys are excellent gas capacitors (Lewis, 1967), suggesting that natural Pd-

157   rich alloys might host significant volumes of trapped gases. To determine He concentrations

158   and the release temperature, Pt–Pd grains were step-heated and measured for He using the

159   MSU-G-01 mass-spectrometric system at IPGG RAS, following the method described in

160   Yakubovich et al. (2017).

161   The decay of ^{238}U, ^{235}U and ^{232}Th can be sources of radiogenic He in Pt minerals in

162   addition to the decay of ^{190}Pt (Shukolyukov et al., 2012b). The degassed Pt–Pd nugget was

163   dissolved in aqua regia at a hot plate for 24 hours. Uranium and Th concentrations were

164   measured in the resulting solutions using a ThermoFisher ELEMENT XR ICP–MS (GEOKHI

165   RAS). Fresh mono-elemental solutions of U and Th (Inorganic Ventures) were used for

166   calibrating the mass spectrometer. The full chemistry blank did not exceed 0.7 ppt both for ^{238}U

167   and ^{232}Th.

168

169   **4. Results**

170   *4.1. Mercury isotopes*

171   Total Hg concentrations and Hg isotopic ratios for Pt–Pd nuggets from Córrego Bom

172   Sucesso are presented in Table 1. Each value refers to a whole-nugget analysis. Value ranges

173   are as follows: $1.05 \leq$ THg $\leq 8.33\%$; $-0.28 \leq \delta^{199}$Hg $\leq -0.09‰$; $-0.14 \leq \delta^{200}$Hg $\leq +0.35‰$; $-$

174    $0.35 \leq \delta^{201}$Hg $\leq +0.25‰$; $-0.25 \leq \delta^{202}$Hg $\leq +0.52‰$. The ranges show consistently negative

175   odd-MIF signals, with Δ^{199}Hg and Δ^{201}Hg between -0.29 and $-0.15‰$, and between -0.28 and

176    $-0.12‰$, respectively. For comparison, plots of δ^{202}Hg vs. Δ^{199}Hg (Fig. 3A) and Δ^{201}Hg vs.

177   Δ^{199}Hg (Fig. 3B) for the Bom Sucesso Pt–Pd nuggets are shown together with data for sulfide

178   and sulfosalt minerals from sediment-hosted Pb–Zn deposits in south-western China (Xu et al.,

179   2018). Those minerals display trends that marginally overlap with the Pt–Pd nuggets, which

180   have a more restricted distribution without any trend (Fig. 3).

181

4.2. Helium isotopes

183   Helium concentrations in Pt–Pd nuggets differ by nearly an order of magnitude, from 3

184   to 19 x 10^{16} at/g (Table 2). Step-heating experiments showed that most of the ^{4}He release

185   occurred above 1000°C with distinct peaks at 1200, 1300 and 1400°C (Fig. 4). The ^{3}He/^{4}He of

186   1.9 ± 0.8 x 10^{-9} (0.0014 ± 0.0005 R_a, using the standard air normalisation) is indicative of a

187   purely radiogenic He origin. This nugget has U and Th contents that are below the detection

188   limit, corresponding to less than 45 ppb U and 25 ppb Th.

189

190   **5. Discussion**

191   *5.1. Constraints on the origin of the Bom Sucesso Pt–Pd nuggets*

192   A local magmatic source of Pt and Pd has been advanced by Reith et al. (2019).

193   Negligible Hg-MIF signals – i.e., Δ^{199}Hg and Δ^{201}Hg of ~0‰ – have been observed in mantle

194   materials in the Guaymas Basin sea-floor rift (Shermen et al., 2009). The significantly negative

195   Δ^{199}Hg and Δ^{201}Hg of our samples (Table 1) rules out a mantle-derived source for the Hg, either

196   directly transferred from a silicate magma or leached from mafic rocks. By extension, the

197   nugget-forming precious metals Pt and Pd are unlikely to have been sourced from a mantle-

198   derived magma, such as Mesozoic dolerite intrusions in the Espinhaco Supergroup. This is

199   confirmed by the He isotopic data, which provide no indication of a contribution of mantle-

200   derived ^{3}He, which is found in modern and ancient hydrothermal mineralisation associated with

201   magmatism (e.g., Stuart et al. 1994, 1995).

202   Further constraints can be placed on the Bom Sucesso Pt–Pd nuggets by the ratio

203   Δ^{199}Hg/Δ^{201}Hg, which has been used to identify pathways of Hg isotopic fractionation. For

204   example, sulfide and sulfosalt minerals from hydrothermal deposits display Δ^{199}Hg/Δ^{201}Hg

205   ~1.0 (Xu et al., 2018; Deng et al., 2021), which is close to that reported from experimental

206   photoreduction of aqueous Hg(II) (Bergquist and Blum, 2007). The Pt–Pd nuggets have odd-

207   MIF signals that are distributed along the Δ^{199}Hg/Δ^{201}Hg line of 1.0 (Fig. 3B), suggesting that

208 the MIF was driven by aqueous Hg(II) photoreduction. On the other hand, the Pt–Pd nuggets

209 appear to have been formed by microbial mediation (Reith et al., 2019; Cabral et al., 2021).

210 Microbial reduction of aqueous Hg(II) has experimentally induced mass-dependent

211 fractionation only, leading to isotopically lighter Hg(0) (Kritee et al., 2007). The data dispersion

212 in Figure 3A likely reflects nugget-forming microbial reduction of aqueous Hg(II) with odd-

213 MIF signals, mostly from photochemical reduction.

214   The negative odd-MIF signal of photochemical reduction requires that the Hg in the Pt–

215 Pd nuggets was exposed to sunlight. Two pathways are possible: (i) supergene solutions carried

216 Hg from the surface to the site of nugget formation within the placer deposit; or (ii) Hg-bearing

217 hydrothermal minerals with the odd-MIF signal were dissolved to release Hg and also Pt and

218 Pd to form nuggets at depth. The reconnaissance He isotopic data rule out the first possibility,

219 according to the following lines of evidence: (i) the ^{3}He/^{4}He in the Pt–Pd nugget is three orders

220 of magnitude lower than the atmospheric ratio; (ii) the high He content of the nugget would

221 require the incorporation of ~3 g of air-equilibrated water into the 2.3-mg nugget; (iii) if all the

222 nugget ^{4}He originated from the in situ decay of ^{190}Pt, the nugget would have unrealistic Pt–He

223 ages (60–340 Ga).

224   Assuming a ^{190}Pt–^{186}Os age of 181 Ma (Cabral et al., 2021), less than 2% of the ^{4}He

225 released from the Pt–Pd nuggets could be derived from in situ radiogenic decay of U and Th,

226 implying that the nugget-trapped He comes from an external source. Low ^{3}He/^{4}He ratios are

227 typical of aquifers in Li-poor (<15 µg/g Li) crustal rocks (e.g., Castro, 2004). The He isotopic

228 data are compatible with Pt–Pd nuggets at least having interacted with old fluids that had

229 previously equilibrated with U- and Th-rich, Li-poor bedrock. Possible source rocks include

230 the quartzite-dominated metasedimentary sequence of the southern Serra do Espinhaço. In the

231 cratonic region west of the southern Serra do Espinhaço, faults that cut the Archaean and

232 Palaeoproterozoic basement and supracrustal rocks are thought to drain deep-seated hydrogen

233 and He (Donzé et al., 2020).

9

234   Cosmogenic ^{3}He can be used to estimate the residence time of nuggets in alluvial

235 systems. Assuming that all ^{3}He in the Pt–Pd nugget is cosmogenic in origin (7 x 10^7 at/g), and

236 using a previously determined cosmogenic ^{3}He production rate in Pt nuggets (Yakubovich et

237 al., 2019), it is inferred that the Pt–Pd nuggets from Córrego Bom Sucesso resided in the placer

238 deposit for less than 2.5 Ma. This rough estimate is close to the residence of detrital Pt grains

239 in the Uorgalan-Kondyor and Is-Turinsk placer deposits (5–28 Ma, Yakubovich et al., 2021).

240   The significant discrepancy between the nugget Pt–Os age of ca. 180 Ma and the ^{3}He-

241 exposure estimate of <2.5 Myr excludes the possibility of nugget formation in the surface

242 environment – i.e., in the Bom Sucesso placer deposit. The depth at which the Pt–Pd nuggets

243 formed can be estimated from the mean denudation rate, determined by cosmogenic ^{10}Be

244 produced in alluvial sediments on the quartzite substratum of the Diamantina region. The mean

245 denudation rate of 4.4 m/Ma (Barreto et al., 2013), combined with the nugget Pt–Os age,

246 suggests that they formed at approximately 800 m below the surface. This is in line with

247 thermochronological modeling using apatite-fission-track (AFT) data from basement granitic-

248 gneissic rocks (Amaral-Santos et al., 2019). The AFT thermal modeling indicates that the

249 temperature at about 800 m below the surface 180 Ma ago was approximately 70°C. It is likely

250 that at this depth the groundwater reached quartzite-hosted hydrothermal veins with high

251 concentrations of Pt–Pd–Hg-bearing minerals, having replaced them in situ. The replacement

252 would have involved removal of more soluble metals, such as As, Sb and Se, and relative

253 enrichment of Pt, Pd and Hg. Alternatively, the groundwater could have obtained its metal load

254 from the dissolution of Pt–Pd–Hg-bearing minerals in nearby hematite–quartz veins. In both

255 scenarios, the estimated groundwater depth is within the conditions under which microbial life

256 would have existed to account for the presence of iodine and organic matter remains in the Bom

257 Sucesso Pt–Pd nuggets, and their Se isotopic values (Cabral et al., 2021).

258

259 *5.2. Mercury recycling and geotectonic implication*

260   These new constraints on the origin of the Bom Sucesso Pt–Pd nuggets indicate that the

261 Hg isotopic signature was inherited from earlier vein minerals that contained recycled Hg from

262 the continental crust. The negative Δ^{199}Hg values for the Pt–Pd nuggets are typical of terrestrial

263 Hg (Blum et al., 2014). Photoreduction of Hg(II) generates negative Δ^{199}Hg in the product

264 gaseous Hg(0), and positive Δ^{199}Hg in the residual Hg(II) phase (Bergquist and Blum, 2007).

265 For this reason, terrestrial pools – e.g., soil and vegetation – mainly show negative Δ^{199}Hg due

266 to the primary accumulation of Hg(0), whereas the ocean pools – e.g., marine sediments and

267 seawater – mainly show positive Δ^{199}Hg because of wet deposition of Hg(II) (Blum et al., 2014).

268 Once acquired in surface reservoirs, MIF signals of Hg isotopes remain even after Hg recycling

269 through subduction zones to form volcanic-arc-related, Hg-bearing epithermal deposits, where

270 inherited positive Δ^{199}Hg values of marine sediments and seawater have been found (Deng et

271 al., 2021). As the seawater Δ^{199}Hg signal is missing in the Pt–Pd nuggets, it seems that Hg was

272 recycled into the hematite–quartz veins from continental sedimentary material. Because the

273 veins are late in relation to the Araçuaí orogen, they likely captured post-orogenic fluids from

274 continental sedimentary rocks. It is interesting to note that the Pt–Pd minerals of hematite–

275 quartz veins have a Hg–As–Sb metal association that is characteristic of low-temperature

276 hydrothermal deposits in a continental setting, such as the Au–Sb deposits of South China with

277 negative Hg-MIF signals (Yin et al., 2019; Fu et al., 2020). If continental sedimentary rocks

278 provided metals for late-orogenic fluids, the veins that resulted from them would have carried

279 Δ^{199}Hg signals of terrestrial surface reservoirs. Our Hg isotopic data support an ensialic setting

280 for Hg cycling, without any traceable contribution of Hg from marine sediments or hydrated

281 oceanic crust, the positive seawater Δ^{199}Hg signal of which can be retrieved from epithermal

282 veins (Deng et al., 2021).

283

284 **6. Conclusion**

285   The Bom Sucesso Pt–Pd nuggets have been taken as examples of supergene

286 accumulation of precious metals within alluvial sediments. This model is too simple. Our Hg

287 and He isotopic data indicate that the nuggets formed in the subsurface, in an environment

288 dominated by ancient groundwater. The nuggets symbolise precious-metal recycling, which is

289 tracked by the odd-MIF signal of Hg isotopes, captured at Earth's surface and kept through

290 diagenesis, metamorphism, orogenesis and fluid overprint.

291

298

299 **References**

300 Aiglsperger, T., Proenza, J. A., Font-Bardia, M., Baurier-Aymat, S., Galí, S., Lewis, J. F.,

301   Longo, F., 2017. Supergene neoformation of Pt–Ir–Fe–Ni alloys: multistage grains explain

302   nugget formation in Ni-laterites. Miner. Deposita 52, 1069–1083.

303 Alkmim, F.F., Kuchenbecker, M., Reis, H.L.S., Pedrosa-Soares, A.C., 2017. The Araçuaí belt,

304   in: Heilbron, M., Cordani, U., Alkmim F. (Eds.), São Francisco Craton, Eastern Brazil.

305   Regional Geology Reviews. Springer, Cham, doi: 10.1007/978-3-319-01715-0_14.

306 Amaral-Santos, E., Jelinek, A.R., Almeida-Abreu, P.A., Genezine, and F.A., 2019. Phanerozoic

307   cooling history of Archean/Paleoproterozoic basement in the southern Espinhaço Range,

308   southeastern Brazil, through apatite fission-track analysis. J. S. Am. Earth Sci. 96, 102352.

309 Barreto, H.N., Varajão, C.A.C., Braucher, R., Bourlès, D.L., Salgado, A.A.R., Varajão,

310   A.F.D.C., 2013. Denudation rates of the Southern Espinhaço Range, Minas Gerais, Brazil,

311   determined by in situ-produced cosmogenic beryllium-10. Geomorphology 191, 1–13.

312 Bergquist, B.A., Blum, J.D., 2007. Mass-dependent and -independent fractionation of Hg

313   isotopes by photoreduction in aquatic systems. Science 318, 417–420.

314 Blum, J.D., Bergquist, B.A., 2007. Reporting of variations in the natural isotopic composition

315   of mercury. Anal. Bioanal. Chem. 388, 353–359.

316 Blum, J.D., Johnson, M.W., 2017. Recent developments in mercury stable isotope analysis.

317   Rev. Mineral. Geochem. 82, 733–757.

318 Blum, J.D., Sherman, L.S., Johnson, M.W., 2014. Mercury isotopes in earth and environmental

319   sciences. Annu. Rev. Earth Planet. Sci. 42, 249–269.

320 Bowles, J.F.W., Suárez, S., 2021. The formation of alluvial platinum-group minerals: present

321   knowledge and the way ahead. Mineral. Mag. 85, 12–21.

322 Cabral, A.R., Lehmann, B., Tupinambá, M., Schlosser, S., Kwitko-Ribeiro, R., de Abreu, F. R.,

323   2009. The platiniferous Au–Pd belt of Minas Gerais, Brazil, and genesis of its botryoidal Pt–

324   Pd–Hg aggregates. Econ. Geol. 104, 1265–1276.

325 Cabral, A.R., Tupinambá, M., Zeh, A., Lehmann, B., Wiedenbeck, M., Brauns, M., Kwitko-

326   Ribeiro, R., 2017. Platiniferous gold–tourmaline aggregates in the gold–palladium belt of

327   Minas Gerais, Brazil: implications for regional boron metasomatism. Mineral. Petrol. 111,

328   807–819.

329 Cabral, A.R., Zack, T., König, S., Eickmann, B., Kwitko-Ribeiro, R., Tupinambá, M.,

330   Lehmann, B., 2019. Distinguishing high- from low-temperature platinum nuggets through

331   their trace-element pattern. Econ. Geol. 114, 201–206.

332 Cabral, A.R., Zeh, A., Tupinambá, M., Pimenta, J., 2020. First evidence for Neoproterozoic

333   magmatism in the Quadrilátero Ferrífero of Minas Gerais, Brazil, and geotectonic

334   implications. J. S. Am. Earth Sci. 104, 102844.

335   Cabral, A.R., König, S., Eickmann, B., Brauns, M., Tupinambá, M., Lehmann, B., Varas-Reus,

336   M. I., 2021. Extreme fractionation of selenium isotopes and possible deep biospheric origin

337   of platinum nuggets from Minas Gerais, Brazil. Geology, doi:10.1130/G49088.1.

338   Carracedo, A., Rodés, Á., Smellie J., Stuart, F.M., 2019. Episodic erosion in West Antarctica

339   inferred from cosmogenic ^{3}He and ^{10}Be in olivine from Mount Hampton. Geomorphology

340   327, 438–445.

341   Cassedanne, J.P., Alves, J.N., 1992. Palladium and platinum from Córrego Bom Sucesso,

342   Minas Gerais, Brazil. Mineral. Rec. 23, 471–474.

343   Cassedanne, J.P., Jedwab, J., Alves, J.N., 1996. Apport d'une prospection systématique à

344   l'étude de l'origine de l'or et du platine alluviaux du Córrego Bom Sucesso (Serro – Minas

345   Gerais). An. Acad. Bras. Ciê. 68, 569–582.

346   Castro, M.C., 2004. Helium sources in passive margin aquifers—new evidence for a significant

347   mantle ^{3}He source in aquifers with unexpectedly low in situ ^{3}He/^{4}He production. Earth

348   Planet. Sci. Lett. 222, 897–913.

349   Chaves, A.d.O., Correia Neves, J.M., 2005. Radiometric ages, aeromagnetic expression, and

350   general geology of mafic dykes from southeastern Brazil and implications for African–South

351   American correlations. J. S. Am. Earth Sci. 19, 387–397.

352   Chemale Jr., F., Dussin, I.A., Alkmim, F.F., Martins, M.S., Queiroga, G., Armstrong, R.,

353   Santos, M.N., 2012. Unravelling a Proterozoic basin history through detrital zircon

354   geochronology: The case of the Espinhaço Supergroup, Minas Gerais, Brazil. Gondwana

355   Res. 22, 200–206.

356   Cousins, C.A., Kinloch, E.D., 1976. Some observations on textures and inclusions in alluvial

357   platinoids. Econ. Geol. 71, 1377–1398.

358   Deng, C., Sun, G., Rong, Y., Sun, R., Sun, D., Lehmann, B., Yin, R., 2021. Recycling of

359   mercury from the atmosphere-ocean system into volcanic-arc–associated epithermal gold

360   systems. Geology, 49, 309-313.

361 Donzé, F.-V., Truche, L., Namin, P.S., Lefeuvre, N., Bazarkina, E.F., 2020. Migration of

362   natural hydrogen from deep-seated sources in the São Francisco basin, Brazil. Geosciences.

363   10, 346.

364 Estrade, N., Carignan, J., Sonke, J.E., Donard, O.F.X., 2009. Mercury isotope fractionation

365   during liquid–vapor evaporation experiments. Geochim. Cosmochim. Acta 73, 2693–2711.

366 Fossen, H., Cavalcante, C., Konopásek, J., Meira, V.T., de Almeida, R.P., Hollanda, M.H.B.M.,

367   Trompette, R., 2020. A critical discussion of the subduction-collision model for the

368   Neoproterozoic Araçuaí-West Congo orogen. Precambrian Res. 343, 105715.

369 Fu, S., Hu, R., Yin, R., Yan, J., Mi, X., Song, Z., Sullivan, N.A., 2020. Mercury and in situ

370   sulfur isotopes as constraints on the metal and sulfur sources for the world's largest Sb

371   deposit at Xikuangshan, southern China. Miner. Deposita 55, 1353–1364.

372 Hattori, K., Cabri, L.J., 1992. Origin of platinum-group-mineral nuggets inferred from an

373   osmium-isotope study. Can. Mineral. 30, 289–301.

374 Hussak, E., 1906. Über das Vorkommen von Palladium und Platin in Brasilien. Z. prakt. Geol.

375   14, 284–293.

376 Kritee, K., Blum, J.D., Johnson, M.W., Bergquist, B.A., Barkay, T., 2007. Mercury stable

377   isotope fractionation during reduction of Hg (II) to Hg (0) by mercury resistant

378   microorganisms. Environ. Sci. Technol. 41, 1889–1895.

379 Lewis, F.A., 1967. The Palladium Hydrogen System. Academic Press, New York, 178 p.

380 Mamyrin, B.A., Tolstikhin, I.N., 1984. Helium Isotopes in Nature. Elsevier, Amsterdam, 274

381   p.

382 Matsuda, J.M., Matsumoto, T.M., Sumino, H.S., Nagao, K.N., Yamamoto, J.Y., Miura, Y.M.,

383   Kaneoka, I.K., Takahata, N.T., Sano, Y.S., 2002. The ^{3}He/^{4}He ratio of the new internal He

384   standard of Japan (HESJ). Geochem. J. 36, 191–195.

385 Oberthür, T., Melcher, F., Weiser, T.W., 2017. Detrital platinum-group minerals and gold in

386   placers of southeastern Samar Island, Philippines. Can. Mineral. 55, 45–62.

387 Reith, F., Nolze, G., Saliwan-Neumann, R., Etschmann, B., Kilburn, M.R., Brugger, J., 2019,

388   Unraveling the formation histories of placer gold and platinum-group mineral particles from

389   Córrego Bom Sucesso, Brazil: A window into noble metal cycling. Gondwana Res. 76, 246–

390   259.

391 Sherman, L.S., Blum, J.D., Nordstrom, D.K., McCleskey, R.B., Barkay, T., Vetriani, C., 2009.

392   Mercury isotopic composition of hydrothermal systems in the Yellowstone Plateau

393   volcanic field and Guaymas Basin sea-floor rift. Earth Planet. Sci. Lett. 279, 86–96.

394 Shukolyukov, Y.A., Yakubovich, O.V., Yakovleva, S.Z., Sal'nikova, E.B., Kotov, A.B., Rytsk,

395   E.Y., 2012a. Geothermochronology based on noble gases: III. Migration of radiogenic He

396   in the crystal structure of native metals with applications to their isotopic dating. Petrol.

397   20, 1–20.

398 Shukolyukov, Y.A., Yakubovich, O.V., Mochalov, A.G., Kotov, A.B., Sal'nikova, E.B.,

399   Yakovleva, S.Z., Korneev, S.I., Gorokhovskii, B.M., 2012b. New geochronometer for the

400   direct isotopic dating of native platinum minerals (^{190}Pt–^{4}He method). Petrol. 20, 491–505.

401 Stuart, F.M., Turner, G., Duckworth, R C., Fallick, A. E., 1994. Helium isotopes as tracers of

402   trapped hydrothermal fluids in ocean-floor sulfides. Geology 22, 823–826.

403 Stuart, F.M. Burnard, P., Taylor R., Turner G., 1995. Resolving mantle and crustal contributions

404   to ancient hydrothermal fluids: He–Ar isotopes in fluid inclusions from Dae Hwa W–Mo

405   mineralisation, South Korea. Geochim. Cosmochim. Acta 59, 4663–4673.

406 Stuart, F.M., Harrop, P.J., Knott, S., Turner, G., 1999. Laser extraction of helium isotopes from

407   Antarctic micrometeorites: Source of He and implications for the flux of extraterrestrial

408   ^{3}He to Earth. Geochim. Cosmochim. Acta 93, 2653–2665.

409 Wollaston, W.H., 1809. On platina and native palladium from Brasil. Philos. Trans. Royal Soc.

410   99, 189–194.

411 Xu, C., Yin, R., Peng, J., Hurley, J.P., Lepak, R.F., Gao, J., Feng, X., Hu, R., Bi, X., 2018. Mercury isotope constraints on the source for sediment-hosted lead-zinc deposits in the Changdu area, southwestern China. Miner. Deposita 53, 339–352.

414 Yakubovich, O.V., Shukolyukov, Y.A., Kotov, A.B., Yakovleva, S.Z., Sal'nikova, E.B., 2010. Geothermochronology based on noble gases: II. Stability of the (U–Th)/He isotope system in zircon. Petrol. 18, 579–594.

417 Yakubovich, O.V., Stuart, F.M., Nesterenok, A.V., Carracedo, A., 2019. Cosmogenic ^{3}He in alluvial metal and alloy grains: Assessing the potential for quantifying sediment transport times. Chem. Geol. 517, 22–33.

420 Yakubovich, O., Stuart, F.M., Mochalov, A., Palamarchuk, R., 2021. Cosmogenic ^{3}He in detrital Pt-alloy grains: tracing the accumulation of critical metals. EGU General Assembly Conference Abstracts, EGU21-10247.

423 Yin, R., Krabbenhoft, D.P., Bergquist, B.A., Wang, Z., Lepak, R.F., Hurley, J.P., 2016. Effects of mercury and thallium concentrations on high precision determination of mercury isotope composition by Neptune Plus multiple collector inductively coupled plasma mass spectrometry. J. Anal. At. Spectrom. 31, 2060–2068.

427 Yin, R., Deng, C., Lehmann, B., Sun, G., Lepak, R.F., Hurley, J.P., Zhao, C., Xu, G., Tan, Q., Xie, Z., Hu, R., 2019. Magmatic-hydrothermal origin of mercury in Carlin-style and epithermal gold deposits in China: evidence from mercury stable isotopes. ACS Earth Space Chem., 3, 1631–1639.

431 Zheng, W., Hintelmann, H., 2010. Nuclear field shift effect in isotope fractionation of mercury during abiotic reduction in the absence of light. J. Phys. Chem. A 114, 4238–4245.

433

Caption to Figures

Fig. 1. The platiniferous gold–palladium belt of Minas Gerais (Cabral et al., 2009, and references therein). The belt is defined by the distribution of lode and platiniferous placer deposits, which are located along the roughly north–south-trending trace of the Brasiliano thrust faults – i.e., the Araçuaí orogen. Data source for ages are given in Cabral et al. (2017). Abbreviations: C. = Córrego (stream); Faz. = Fazenda (farm); Fm. = Formation; Gr. = Group; Sg. = Supergroup

Fig. 2. Backscattered-electron images of Pt–Pd nuggets from Córrego Bom Sucesso. A. Botryoidal, arborescent aggregate. B. Concentric Pt–Pd layers on a hollow core of botryoidal moulds.

**Fig. 3.** Plots of $\delta^{202}Hg$ vs. $\Delta^{199}Hg$ (A) and $\Delta^{201}Hg$ vs. $\Delta^{199}Hg$ (B) for the Bom Sucesso Pt–Pd nuggets. For comparison, sulfide and sulfosalt minerals from sediment-hosted lead–zinc deposits in south-western China are also plotted (Xu et al., 2018). Those hydrothermal minerals likely incorporated the Hg-isotope MIF from the metamorphic country rocks, which preserved surface MIF signals from terrestrial environments (negative odd-MIF values). Crosses refer to analytical uncertainties – i.e., 2SD values in reference materials, Table 1).

Figure 4. Kinetics of thermodesorption of ^{4}He from a fragment of Pt–Pd nugget (0.183 mg). Duration of each step of heating was 280 seconds.
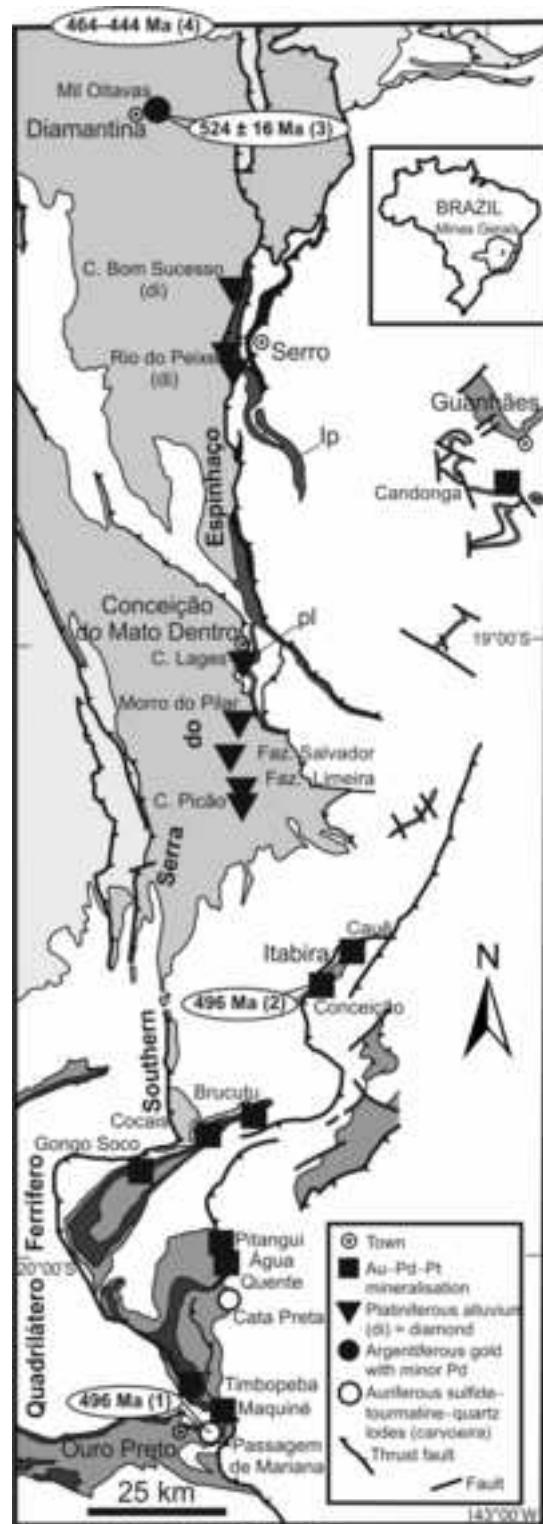
Figure 1   Click here to access/download;Figure;renamed_cbb78.jpg
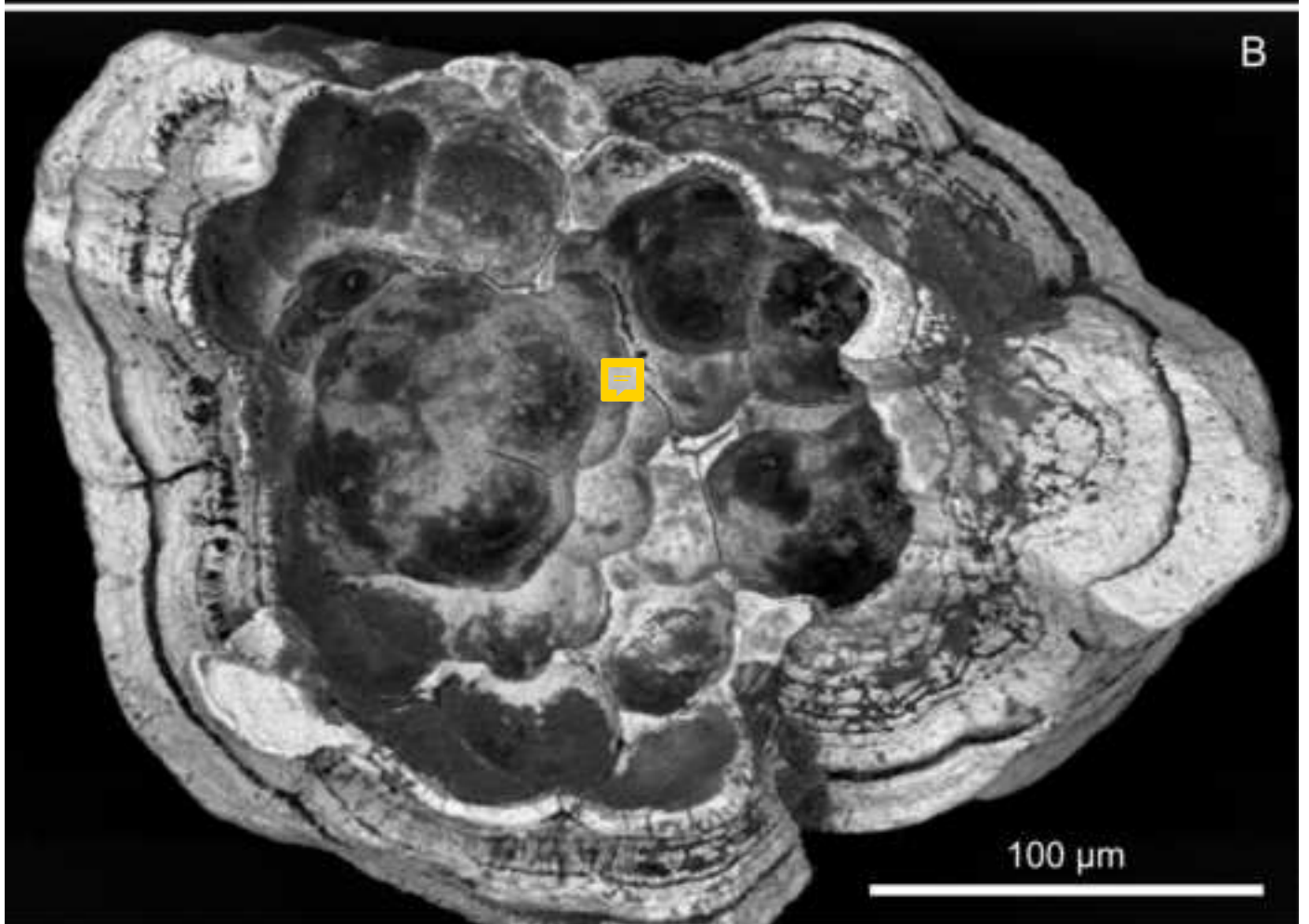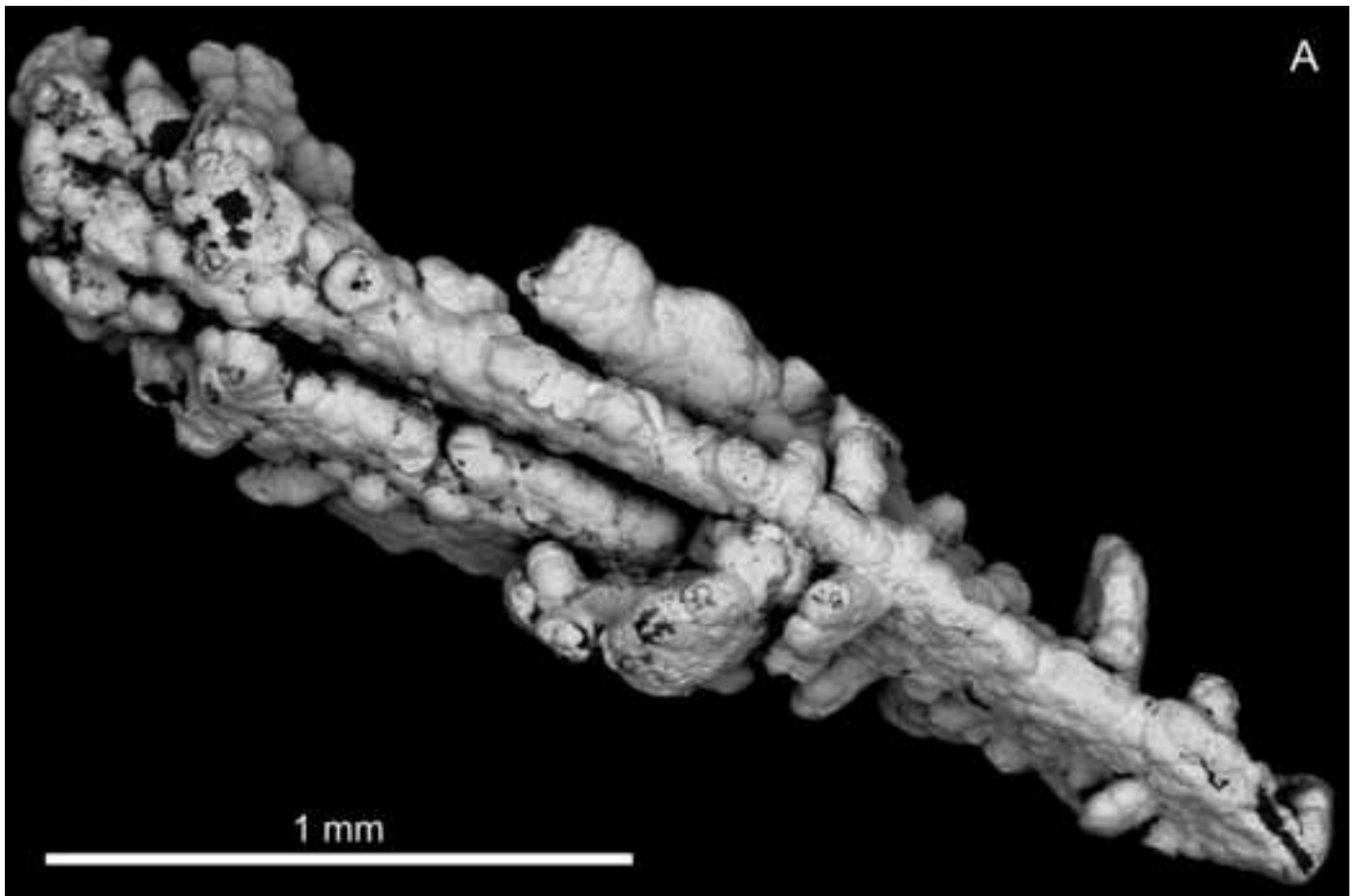
Figure 1

Figure 3

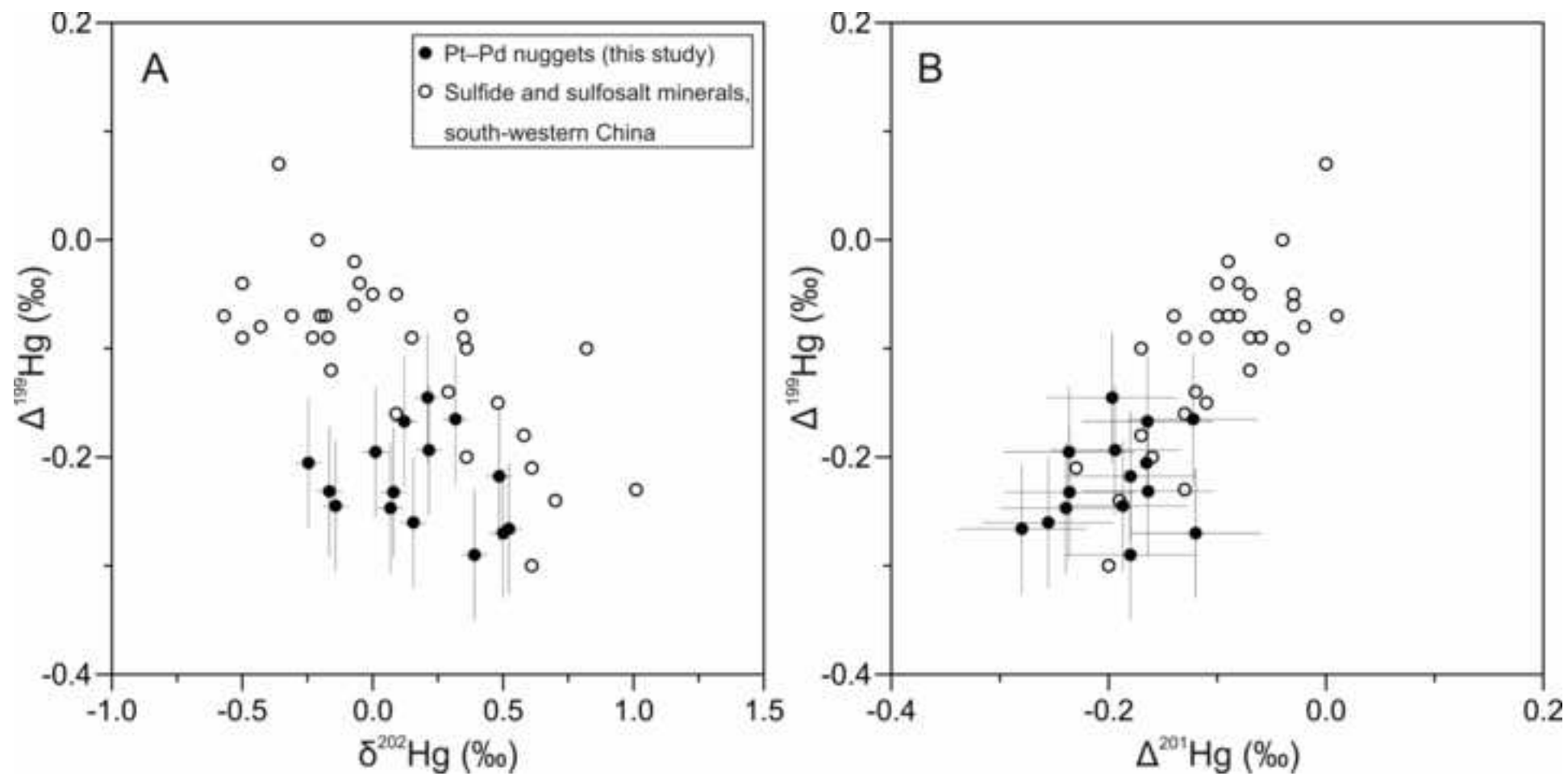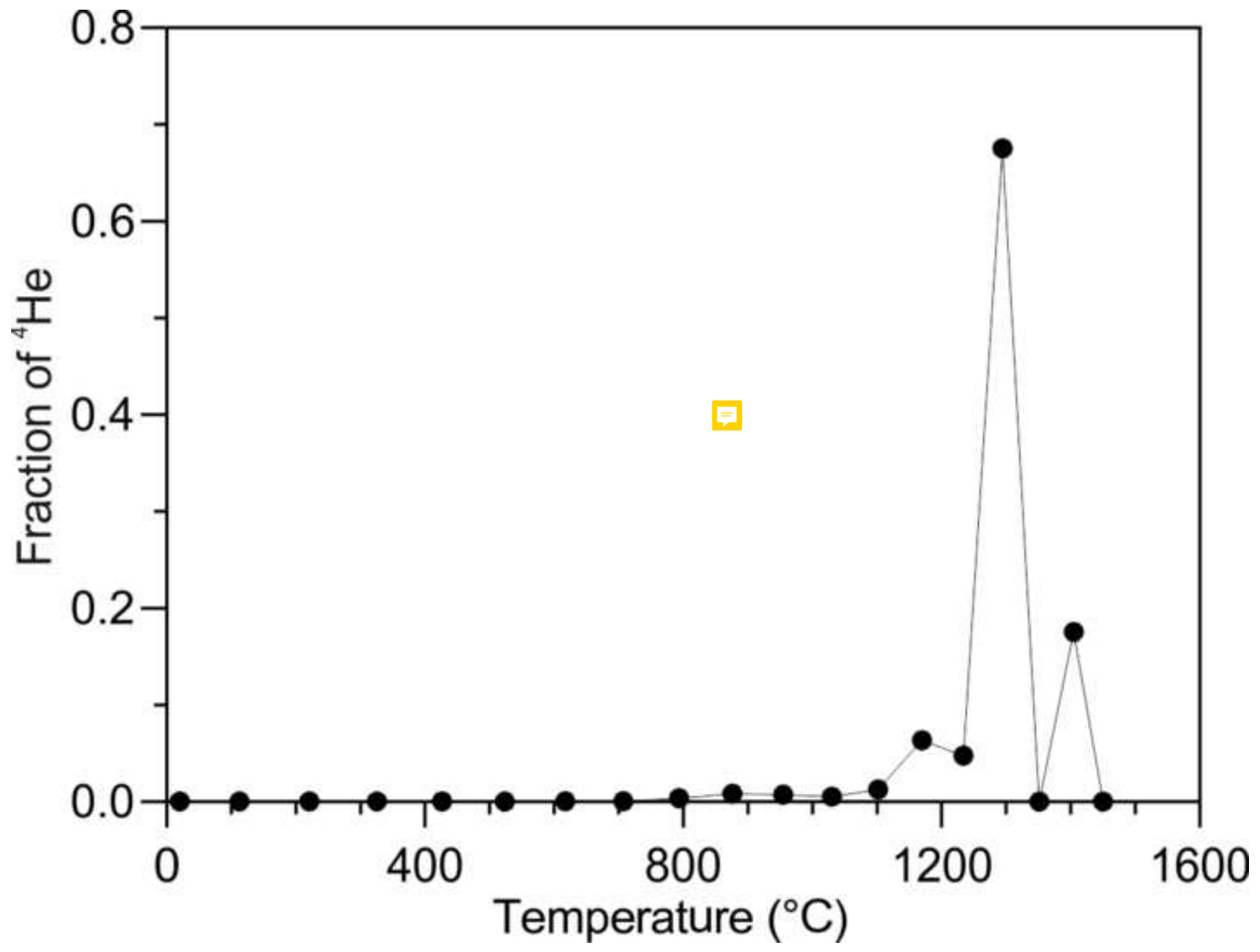Figure 4

Table 1. Results of measurements for Hg isotopes in Pt–Pd nuggets from Córrego Bom Sucesso, Minas Gerais, and in reference materials

	Hg*	δ^{199}Hg	δ^{200}Hg	δ^{201}Hg	δ^{202}Hg	Δ^{199}Hg	Δ^{200}Hg	Δ^{201}Hg
Nugget	(%)	(‰)	(‰)	(‰)	(‰)	(‰)	(‰)	(‰)
1	2.73	-0.19	0.15	0.11	0.39	-0.29	-0.05	-0.18
2	4.35	-0.15	0.35	0.25	0.50	-0.27	0.10	-0.12
3	2.10	-0.19	-0.01	-0.23	0.01	-0.20	-0.01	-0.24
4	8.33	-0.14	0.05	-0.03	0.22	-0.19	-0.06	-0.19
5	1.05	-0.21	0.01	-0.18	0.08	-0.23	-0.03	-0.24
6	3.57	-0.13	0.21	0.11	0.52	-0.27	-0.06	-0.28
7	6.40	-0.22	0.05	-0.14	0.16	-0.26	-0.02	-0.26
8	3.12	-0.28	-0.07	-0.29	-0.14	-0.24	0.00	-0.19
9	7.37	-0.09	0.11	0.12	0.32	-0.16	-0.05	-0.12
10	1.45	-0.14	0.08	-0.07	0.12	-0.17	0.01	-0.16
11	3.63	-0.27	-0.08	-0.29	-0.17	-0.23	0.00	-0.16
12	5.91	-0.09	0.08	-0.04	0.21	-0.15	-0.03	-0.20
13	2.63	-0.27	-0.14	-0.35	-0.25	-0.21	-0.02	-0.17
14	4.91	-0.23	0.10	-0.19	0.07	-0.25	0.06	-0.24
15	1.88	-0.10	0.21	0.18	0.49	-0.22	-0.03	-0.18
Reference material								
	(ng/g)							
GSS-4	590	-0.88	-0.89	-1.72	-1.79	-0.43	0.01	-0.38
GSS-4	590	-0.86	-0.87	-1.74	-1.74	-0.42	0.00	-0.43
GSS-4	590	-0.82	-0.86	-1.76	-1.77	-0.38	0.03	-0.43
Mean		-0.85	-0.87	-1.74	-1.76	-0.41	0.01	-0.41
2SD		0.06	0.04	0.03	0.05	0.06	0.03	0.06
	(ng/mL)							
NIST3177	1	-0.10	-0.24	-0.44	-0.51	0.03	0.02	-0.05
NIST 3177	1	-0.16	-0.25	-0.46	-0.53	-0.03	0.01	-0.06
NIST 3177	1	-0.16	-0.31	-0.43	-0.55	-0.02	-0.03	-0.02
Mean		-0.14	-0.27	-0.44	-0.53	-0.01	0.00	-0.05
2SD		0.06	0.07	0.03	0.04	0.06	0.05	0.04

* Total Hg

Table 2. Results of measurements for He isotopes in Pt–Pd nuggets from Córrego Bom Sucesso, Minas Gerais

Nugget	Mass (mg)	^{4}He $(10^{10}$ at)	1SD	^{3}He $(10^4$ at)	1SD	R/Ra	^{4}He $(10^{16}$ at/g)	1SD
1*	2.272	8700	500	16.0	6.7	0.0014	3.8	0.2
2	0.183	3400	220	-	-	-	18.6	1.3
3	6.05	43500	130		-	-	7.2	0.02
4	0.21	2550	30	-	-	-	12.1	0.33
5	0.28	700	17	-	-	-	2.5	0.07
Hot blank								
SUERC		0.07	0.03	1.50	1.10	17	-	-
IPGG RAS		0.13	0.8	-	-	-	-	-

* Measurement performed at SUERC; all others at IPGG RAS